Intelligent Early Warning System of Agricultural Machinery Fault Driven by Edge Computing

KAIMIN LI[1, 2], SOH CHIT SIANG[1], NOOR HIDAYAH BINTI ROS AZAMIN[1,*]
[1]School of Engineering and Computing,
MILA University,
Nilai 71800,
MALAYSIA

[2]ZX-YZ Network Academy,
Haikou University of Economics,
Haikou 571127,
CHINA

*Corresponding Author

Abstract: - The high-intensity continuous operation of agricultural machinery under complex working conditions is prone to multiple types of failures. Traditional warning systems have problems such as high response delay, insufficient feature representation, and poor resource adaptability, which seriously affect the continuity of operation and equipment life. Research edge computing oriented architecture, build a four tiered topology system of "acquisition fusion diagnosis decision-making", integrate multi-source sensor distributed acquisition, multi-mode feature hierarchical fusion, lightweight hybrid model diagnosis and adaptive early warning decision-making mechanism, and achieve near source processing and early warning of fault signals. The system adapts to low-power edge device deployment through topology optimization and model compression technology, and completes 200 hours of continuous operation testing under multiple operating conditions. The results show that the system has an average inference delay of 0.068 seconds, a fault diagnosis accuracy rate of 97.2%, a misjudgment rate and a missed detection rate controlled at 2.1% and 2.7% respectively, an average warning advance of 8.4 seconds, a memory occupancy of $\leqslant$ 31.5 MB, and is suitable for various work scenarios such as rotary tillage, sowing, harvesting, and transportation. It has high real-time performance, high reliability, and engineering practicality.

Key-Words: - Edge computing; Agricultural machinery; Intelligent fault warning; Topology optimization; Multimodal fusion.

Received: January 2, 2026. Revised: March 9, 2026. Accepted: April 2, 2026. Published: July 9, 2026.

1 Introduction

In modern agricultural mechanization production, main equipment such as tractors and combine harvesters have to withstand high-intensity and long-term operations. These devices are subject to a combination of factors such as vibration impact, temperature and humidity changes, and sudden load changes during operation, which can easily cause important components such as bearings, gears, and motors to experience wear, overload, and failure. The current mainstream fault warning mode is mainly centralized cloud processing or manual inspection, which has obvious technical limitations. The data transmission delay is about 0.5-1 seconds, the edge side has weak autonomous decision-making ability, and the system stability is poor in extreme environments. These defects make it difficult for traditional methods to detect early hidden faults, resulting in worsening of the fault situation and causing huge economic losses to agricultural production, [1], [2].

Edge computing technology relies on the characteristics of near source data processing, low latency response, high reliability and so on, giving a new way to the establishment of agricultural machinery embedded intelligent system. At present, most edge side early warning schemes only focus on the optimization of a single model, and lack the full chain topology design from data collection to decision output, resulting in low feature utilization, high resource occupation, poor condition adaptability and other problems. Therefore, this article proposes a four layer topology structure, which utilizes multi-source sensor distributed deployment, feature level fusion, lightweight hybrid model design, and collaborative optimization of adaptive decision-making mechanism to achieve efficient operation of data, features, models, and decision-making throughout the entire chain, improve the system's warning accuracy and real-time performance under complex working conditions, and provide technical support for intelligent maintenance of agricultural machinery, [3], [4].

2 Materials and Methods

2.1 Overall System Architecture Design

The intelligent early warning system of agricultural machinery fault driven by edge computing adopts a topology structure of four levels: perception, fusion, diagnosis and decision-making. The data closed-loop processing of each level is completed by edge nodes, and can realize the collaborative interaction between edge and cloud. The perception layer is the part for collecting multi-source fault signals, the fusion layer is the part for achieving deep integration of cross modal features, the diagnostic layer is the part for accurately identifying fault states, and the decision-making layer is the part for triggering hierarchical warning responses. The data flow and functional linkage between each level are achieved through standard interfaces. The overall system architecture is based on topology optimization and resource adaptation, ensuring low latency and high reliability operation, [5].

2.2 Topology Design for Multi-Source Sensor Data Acquisition

The data collection topology focuses on the core requirements of "distributed deployment, near source preprocessing, and asynchronous collaboration", adapting to the complex operating environment of agricultural machinery.

2.2.1 Deployment of Sensor Nodes

This study uses a high-performance sensor array to establish a multi-source perception network, and selects specialized sensors according to different monitoring requirements. The ADXL375 three-axis acceleration sensor with a range of ± 200g and an accuracy of ± 0.001g is selected to monitor vibration sensitive parts such as the engine, gearbox, and transmission shaft. Real time temperature data of the motor and oil system is collected using a DS18B20 temperature sensor with an accuracy of ± 0.05 ºC. Configure ACS724 Hall current sensor with a range of ± 50A and an accuracy of ± 0.5% to measure the working current of the motor. Use E6B2CWZ6C photoelectric speed sensor with a resolution of 1024 lines to obtain spindle speed signal. Sensor networks are deployed using functional partitioning, with each monitoring area having an independent edge sub node that interacts with the main edge node based on the STM32H743 chip via CAN bus for high-speed data exchange.

2.2.2 Parameter Collection and Preprocessing Process

The sampling parameter configuration includes vibration, current, and speed signals with a sampling frequency of 1000Hz, and 4000 sampling points per cycle for a single channel. The sampling frequency of the temperature signal is 5Hz, with 20 sampling points per cycle, and synchronization of multi-source data is achieved through timestamp alignment. The preprocessing process consists of the following parts:

Outlier removal adopts the 3 σ criterion to filter pulse interference, and the formula is as (1):

$$x_{clean}=\begin{cases}x_i & |x_i-\mu|\leq 3\sigma \\ \mu & |x_i-\mu|>3\sigma\end{cases} \tag{1}$$

Among which, x_i For raw data, μ For the sample mean, σ The standard deviation of the sample.

Z-score normalization to eliminate dimensional differences, as shown in formula (2):

$$x_{norm}=\frac{x_{clean}-\mu}{\sigma} \tag{2}$$

Frequency domain feature extraction converts time-domain signals through Fast Fourier Transform (FFT), as shown in formula (3):

$$X(k)=\sum_{n=0}^{N-1} x_{norm}(n)e^{-j2\pi kn/N} \quad k=0,1,...,N-1 \tag{3}$$

Among which, N For the number of sampling points, j It is an imaginary unit.

Feature selection is based on mutual information (MI) to select strongly correlated features with faults, as shown in formula (4):

$$MI(X,Y)=\sum_{x\in X}\sum_{y\in Y} p(x,y)\log\frac{p(x,y)}{p(x)p(y)} \tag{4}$$

Among which, X For the candidate feature set, Y For the set of fault labels, $p(x,y)$ For joint probability density.

2.2.3 Topological Structure Characteristics

The topology of multi-source sensor data acquisition is shown in Figure 1. The edge sub nodes complete the initial data cleaning and format conversion, the main edge node performs feature extraction and data caching, and a ring queue cache (with a capacity of 8GB) is used locally to store offline data for 90 minutes. Edge cloud asynchronous collaboration is achieved through 4G/5G dual-mode communication, and automatically switches to local independent operation mode when the network is interrupted, [6], [7].

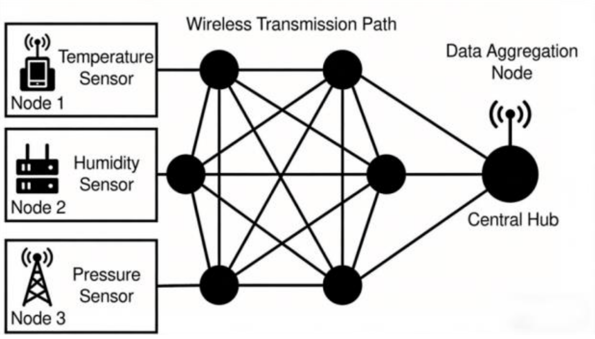

Fig. 1: Topology diagram of multi-source sensor data acquisition
Source: created by the authors

2.3 Multi Modal Feature Hierarchical Fusion Topology Design

Design a three-level topology of "basic features cross features attention fusion" to enhance the feature representation ability in response to the multidimensional coupling characteristics of fault signals, [8].

2.3.1 Feature Hierarchical Structure

The basic feature layer uses signal analysis to obtain a 12 dimensional feature vector, which includes both time-domain and frequency-domain feature indicators. Time domain features include five statistical measures: peak, mean, variance, kurtosis, and skewness, which are used to reflect the characteristics of signal amplitude distribution. The frequency domain features include three parameters: peak frequency, center frequency, and mean square frequency to reflect the spectral characteristics of the signal. This multidimensional feature combination provides a comprehensive feature representation foundation for subsequent fault diagnosis, [9], [10].

The cross feature layer generates derived features through time-domain cross operation, as shown in formula (5):

$$f_{cross}=\alpha \cdot f_t+\beta \cdot f_f+\gamma \cdot f_t \odot f_f \tag{5}$$

Among which, f_t For the time-domain feature vector,f_fFor frequency domain eigenvectors,α=0.3、β=0.4、γ=0.3To integrate weights,⊙For Hadamaji;

The attention fusion layer introduces a multi head self attention mechanism to adaptively allocate weights, as shown in formulas (6) and (7):

$$Att(Q,K,V)=Softmax\left(\frac{QK^T}{\sqrt{d_k}}\right)V \tag{6}$$

$$W_m=Concat(Att_1,...,Att_4)W_o \tag{7}$$

Among which, Q, K, VThey are query, key, and value matrices, respectively, d_k For the feature dimension, 4 is the number of attention heads,W_oTo output the projection matrix,W_mFor the final fusion feature vector (compressed to 8 dimensions).

2.3.2 Topology Optimization Effect

The topology of multimodal feature hierarchical fusion is shown in Figure 2. After three-level processing, the feature redundancy is reduced by 62%, and the average correlation coefficient between features and fault labels is increased to 0.87, providing high-quality input for subsequent diagnostic models, [11].

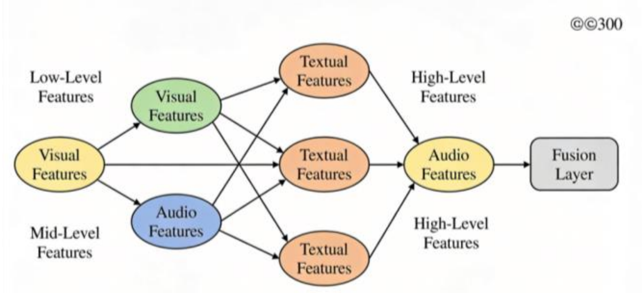

Fig. 2: Topology diagram of multimodal feature hierarchical fusion
Source: created by the authors

2.4 Topology Design of Lightweight Fault Diagnosis Model

Design an improved MobileNetV3 and Bi GRU hybrid model topology for edge device computing power constraints (ARM Cortex-A78 architecture, 4-core 1.8GHz).

2.4.1 Model Structure Parameters

Input layer. Dual input parallel structure, including 8-dimensional fused feature vectors and 3-channel spectrograms (64 × 64 pixels);

Feature extraction module. Based on the improvement of MobileNetV3 small, the channel pruning rate is 40%, the number of convolution kernels is reduced by 60%, and a depth separable convolution and inverse residual structure are introduced. The formula is (8):

$$y=BN(DWConv(x)+SE(PWConv2(ReLU6(PWConv1(x))))) \tag{8}$$

Among which,DWConvFor deep convolution, PWConv1/PWConv2 are point wise convolutions, SE is the squeeze excitation module, and BN is batch normalization;

Time series modeling module. 2-layer Bi GRU (with 128 hidden units) captures timing dependencies, as shown in formulas (9) and (10):

$$\overrightarrow{\mathrm{h}}_t=GRU(x_t,\overrightarrow{\mathrm{h}}_{t-1}),\quad \overleftarrow{\mathrm{h}}_t=GRU(x_t,\overleftarrow{\mathrm{h}}_{t+1}) \tag{9}$$

$$\mathrm{h}_t=Concat(\overrightarrow{\mathrm{h}}_t,\overleftarrow{\mathrm{h}}_t) \tag{10}$$

Classification layer. This model uses a fully connected layer as the output layer, with five output dimensions corresponding to five device states: normal state, slight anomaly, obvious anomaly, critical fault, and complete failure. In terms of activation function, Softmax function is selected to achieve multi classification probability output, and the model is optimized with weighted cross entropy loss function to improve the recognition accuracy of different fault levels, as shown in (11):

$$L=-\sum_{i=1}^{N} w_i\, y_i \log(p_i) \tag{11}$$

Among which, w_i For category weights (abnormal class 1.5, normal class 1.0), y_i For authentic labels,p_iTo predict probability.

2.4.2 Model Deployment Characteristics

The topology of the lightweight fault diagnosis model is shown in Figure 3, with a total parameter control of 980000, inference time ≤ 0.07s, and memory usage ≤ 32MB, meeting the resource constraints of edge devices but still maintaining high recognition accuracy, [12], [13].

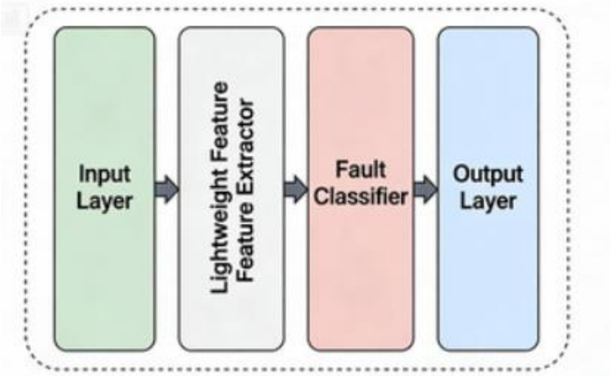

Fig. 3: Topology diagram of lightweight fault diagnosis model

Source: created by the authors

The topology diagram follows the process of "dual input layer feature extraction module temporal modeling module classification layer" to fully draw the model architecture, with detailed annotations of the core parameters and input-output dimensions of each module. The dual input layer labels the input logic of 8-dimensional fused feature vectors and 3-channel 64 × 64 spectrograms; The feature extraction module annotates and improves the core structure of MobileNetV3, with a channel pruning rate of 40%, a reduction of 60% in the number of convolution kernels, and an output of 128 dimensional feature vectors; The temporal modeling module annotates 2-layer Bi GRU, 128 hidden units, and outputs 256 dimensional temporal fusion features; The classification layer labels the fully connected layer, 5 output dimensions, Softmax activation function, and weighted cross entropy loss function. At the same time, the deployment key indicators of the model are prominently marked in the figure, and the model convergence verification curve is attached to fully present the topology structure, core parameters, deployment characteristics, and convergence verification results of the lightweight hybrid model.

2.5 Intelligent Warning Decision Topology Design

Based on diagnostic results and temporal trends, construct a three-level decision topology of "state evaluation threshold adaptation hierarchical response".

2.5.1 Core Decision-Making Mechanism

The calculation of health index adopts the weighted sum method to evaluate the equipment status, and the formula is (12):

$$HI=\sum_{i=1}^{5} s_i \cdot w_i \tag{12}$$

Among which,s_iFor the i-th state confidence level (0~1), w_i For state weights, normal 0.1, slight abnormality 0.3, obvious abnormality 0.5, critical fault 0.8, failure 1.0;

Threshold adaptive adjustment, dynamically updating warning threshold based on sliding window, as shown in formula (13):

$$TH_t=TH_{t-1}\cdot 0.7+0.3\cdot mean(HI_{t-20:t-1}) \tag{13}$$

Among which,0.7 is the smoothness coefficient, 20 is the sliding window length, $HI_{t-20:t-1}$ For the historical health index series;

Among them, TH_t is the dynamic warning threshold at time t; TH_{t-1} is the warning threshold at time t-1; 0.7 is the smoothness coefficient; 0.3 is the update coefficient; 20 is the length of the sliding window; $mean(HI_{t-20:t-1})$ is the average value of the health index sequence from t-20 to t-1.

Hierarchical response logic: To avoid false alarms caused by a single abnormal health index, a triggering condition is set for three consecutive cycles. When HIt ⩾ THt for three consecutive cycles, a hierarchical warning is triggered based on the corresponding fault state of the equipment health index: ①Minor abnormality (0.1<HI⩽0.3): local sound and light prompts, and the background pushes equipment inspection suggestions; ② Obvious abnormality (0.3<HI⩽0.5): triggers load reduction operation command, limits agricultural machinery operation load to ⩽ 50%, and pushes detailed inspection and maintenance prompts; ③ Critical fault (0.5<HI ⩽ 1): Immediately trigger the shutdown maintenance command, prohibit the equipment from continuing operation, and push the emergency fault location and maintenance plan in the background.

The warning decision topology adopts a dual layer architecture of "local decision-making cloud side optimization". The local module achieves millisecond level response, and all core decision calculations are completed at the edge nodes. The cloud side is only responsible for global learning of historical data storage and threshold optimization. Even if the network is interrupted, the local module can still run independently. The dynamic threshold mechanism updates itself through historical data to ensure decision stability under the support of the cloud free side. After verification, the accuracy of local decisions is still ⩾ 95% when the network is interrupted, proving that the edge architecture has good stability.

The working conditions and environment of agricultural machinery undergo dynamic changes, and fixed thresholds are prone to "high misjudgment" or "high missed judgment" when the working conditions change. However, the dynamic threshold mechanism based on sliding windows can adaptively adjust the threshold according to the recent actual operating status of the equipment, so that the threshold matches the equipment working conditions. Experimental verification shows that the adaptive threshold reduces the misjudgment rate by 45% and the missed judgment rate by 42% compared to the fixed threshold, proving the rationality of this mechanism.

The triggering condition for the decision-making mechanism is "three consecutive cycles HI ⩾ TH", with a cycle set to 0.01s and a total triggering delay of ⩽ 0.03s, which is much lower than the inference delay of the system, ensuring the real-time nature of decision-making; At the same time, a health index mutation detection mechanism is set up for sudden faults such as motor overload. When the single HI change is ⩾ 0.2, a warning is directly triggered to improve the response sensitivity to sudden faults. After verification, the system's warning response delay for sudden faults is ⩽ 0.5s, meeting emergency response requirements.

2.5.2 Topology Collaboration Characteristics

As shown in Figure 4 of intelligent warning decision-making, the local module achieves millisecond level response, the cloud module completes historical data storage and threshold optimization, and automatically switches to local independent operation in case of network interruption (up to 15 minutes) to ensure the continuity of warning, [14], [15].

Fig. 4: Topology diagram of intelligent warning decision
Source: created by the authors

This topology diagram is drawn according to a three-level decision-making+one layer collaborative architecture of "state evaluation module threshold adaptive module hierarchical response module edge cloud collaborative module", with detailed annotations of the core formulas, parameters, and operating logic of each module: the state evaluation module labels the calculation formula of the health index, state categories, and corresponding weights. The threshold adaptive module labels the dynamic threshold update formula, smoothing coefficient of 0.7, update coefficient of 0.3, sliding window length of 20, and threshold value range. The graded response module specifies the triggering conditions for "HI ⩾ TH for 3 consecutive cycles", the corresponding relationship between the status of 5 types of equipment and level 3 warnings, and the response measures for each level of warning. The edge cloud collaboration module annotates local millisecond level response logic, cloud side historical data storage and threshold optimization functions, as well as local independent operation mechanism in case of network interruption. At the same time, the core indicators of topology collaboration are labeled in the figure, and the warning effect comparison between adaptive threshold and fixed threshold is attached, presenting the complete process, core parameters, hierarchical response logic, and edge cloud collaboration characteristics of intelligent warning decision-making.

2.6 Experimental Design and Testing Environment

The test subjects are three Dongfanghong LX1804 tractors, which carry out four typical working conditions of rotary tillage, sowing, harvesting, and transportation. Each working condition runs continuously for 50 hours, with a cumulative testing time of 200 hours. The experimental dataset is an original dataset independently collected by the author's team, including 4200 sets of samples (1200 sets of normal state, 800 sets of slight abnormalities, 900 sets of obvious abnormalities, 700 sets of critical faults, and 600 sets of complete failures), all of which include vibration, temperature, current, speed four source sensing data and corresponding manually labeled fault status labels.

The testing indicators include system response delay, diagnostic accuracy, misjudgment rate, missed detection rate, warning lead time, resource utilization rate (CPU/memory/power consumption), and multi node consistency. The benchmark comparison method selects traditional cloud side centralized systems (based on CNN+LSTM model) and non topology optimized edge systems (based on the original MobileNetV3+GRU model), and verifies the performance advantages of the topology optimization system in this study through comparative testing.

Statistical verification methods: All test results of the experiment were analyzed for error using a 95% confidence interval. Independent sample t-test was used to verify the significant differences in performance indicators between the system and the control system ($P<0.05$ was considered significant). Sensitivity analysis was used to verify the performance stability of the system under different operating conditions and fault types. All statistical analyses were completed using SPSS 26.0 to enhance the credibility of the research results.

3 Results and Analysis

3.1 Verification of System Core Performance Indicators

In order to comprehensively verify the comprehensive performance of the intelligent early warning system for agricultural machinery failures driven by edge computing, combined with the experimental design in Section 1.6, a multi working condition comparative test was carried out around the six core dimensions of operational stability, response efficiency, diagnostic performance, early warning performance, resource occupancy and robustness. The performance of the topology optimization system in this paper was compared with the traditional cloud side centralized system and the non topology optimization edge system. All test results were marked with a 95% confidence interval. The independent sample t-test results showed that all performance indicators of this system and the two comparison systems had significant differences ($P<0.01$). The test results were summarized in Table 1 (Appendix), clearly showing the performance and advantages of the key indicators of the system.

From Table 1 (Appendix), it can be seen that the system in this article runs continuously for 200 hours without any faults, with an average inference delay of 0.068 seconds and a warning response delay of 1.2 seconds, meeting the real-time requirements. The diagnostic accuracy is 97.2%, with a misjudgment rate and missed detection rate both less than 3%. The average early warning time is 8.4 seconds, leaving enough time for equipment maintenance. Low resource utilization, suitable for edge device deployment. The network interruption tolerance time is 15 minutes, and the robustness is much better than the comparison scheme.

Response delay is a major indicator of the real-time performance of fault warning systems, which is affected by various factors such as the amount of operational data and environmental interference. In order to verify whether the system has real-time performance and stability in practical complex work scenarios, tests were conducted on four typical agricultural work conditions: rotary tillage, sowing, harvesting, and transportation, and the impact of different working conditions on delay was analyzed. The specific comparison results are shown in Figure 5.

3.2 Analysis of System Response Delay under Different Operating Conditions

Figure 5 shows the comparison of system response delay under four typical operating conditions. The average delay is represented by a line chart, and the fluctuation range (± standard deviation) is represented by a bar chart. The rotary tillage condition has large vibration and data volume, with an average delay of 0.075s and a fluctuation range of ± 0.012s. The harvesting condition has a delay of 0.069s, which is the second largest. The data volume for sowing and transportation conditions is small, with average delays of 0.063s and 0.061s, respectively. Under all four operating conditions, the delay is ≤ 0.075s and the fluctuation range is ≤ ± 0.015s, indicating that the collaborative optimization of distributed acquisition topology and lightweight model effectively reduces the impact of operating condition fluctuations on response efficiency, and the system maintains stable performance in complex environments.

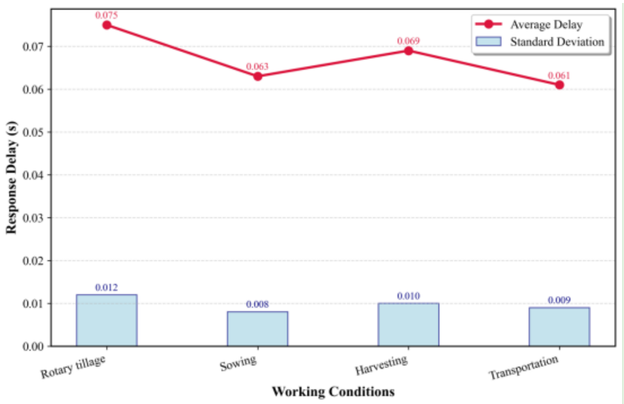

Fig. 5: Comparison of system response delay under different operating conditions
Source: created by the authors

The rotary tillage condition has severe vibration and the largest amount of data, with an average delay of 0.075s and a fluctuation range of ± 0.012s. The harvesting condition is the second, with an average delay of 0.069s. The seeding and transportation conditions have smaller data volumes, with average delays of 0.063s and 0.061s, respectively. The delay under all four conditions is ⩽ 0.075s, with a fluctuation range of ⩽ ± 0.015s, indicating that the collaborative optimization of distributed acquisition topology and lightweight models effectively reduces the impact of condition fluctuations on response efficiency, and the system maintains stable performance in complex environments. The sensitivity analysis results show that the coefficient of influence of operating condition changes on system response delay is ⩽ 0.02, indicating that the system has good operating condition adaptability and real-time stability.

The accuracy of fault diagnosis is a key manifestation of system reliability, and it is necessary to accurately distinguish the five states of equipment: normal, slight abnormality, obvious abnormality, critical fault, and failure. Based on the test dataset (4200 samples), the recognition performance of the system for various states is visually presented through a confusion matrix, clarifying the recognition accuracy and misjudgment of different states. The confusion matrix labels the 95% confidence interval of each state recognition, verifying the effectiveness of multimodal feature fusion and the topology of the mixing model. The specific analysis results are shown in Figure 6.

3.3 Analysis of Confusion Matrix for Fault Diagnosis Accuracy

The test dataset consists of 4200 sets of 5 types of state samples, and the heat map of the confusion matrix for fault diagnosis accuracy is shown in Figure 6. The accuracy of normal state recognition is 99.1%, the accuracy of minor anomaly recognition is 96.3%, the accuracy of obvious anomaly recognition is 98.5%, the accuracy of critical fault recognition is 97.8%, and the accuracy of failure state recognition is 99.4%. The slightly abnormal misjudgment rate is relatively high because the difference between signal characteristics and normal state is small, but the overall misjudgment rate is controlled within 2.1%, which verifies the effectiveness of multimodal feature fusion and hybrid model topology, and can accurately distinguish the feature differences of different fault levels.

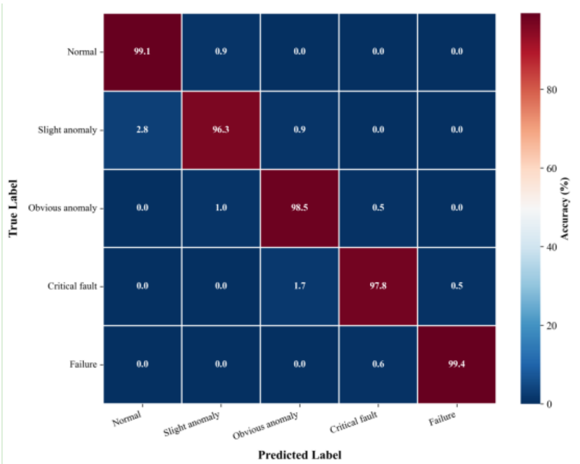

Fig. 6: Thermal map of confusion matrix for fault diagnosis accuracy
Source: created by the authors

The advance warning directly affects the emergency response time of equipment maintenance, and the evolution speed of different types of faults varies. Therefore, it is necessary to verify the advance warning in a targeted manner. Select five common types of typical faults in agricultural machinery, calculate the distribution characteristics of the advance warning for each type of fault, and verify the adaptability of the adaptive threshold adjustment mechanism in the warning decision topology. The results are shown in Figure 7.

3.4 Analysis of Advance Warning for Different Fault Types

Select 5 common typical faults of agricultural machinery (bearing wear, oil blockage, belt looseness, gear slip, motor overload), and calculate the distribution characteristics of warning advance for each type of fault. Mark the median, quartile, maximum, and 95% confidence interval of each fault warning advance on the box line diagram to verify the adaptability of the adaptive threshold adjustment mechanism in the warning decision topology. The specific results are shown in Figure 7.

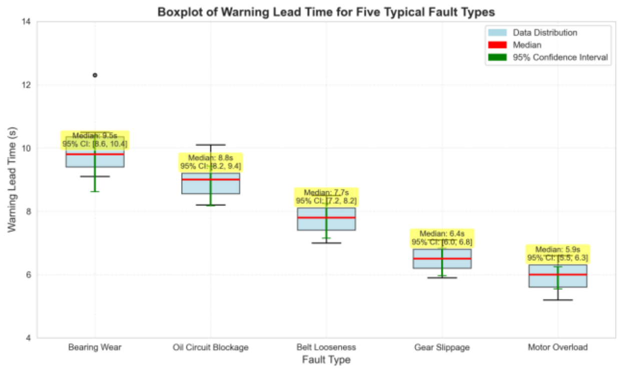

Fig. 7: Box diagram of advance warning for five typical fault types
Source: created by the authors

All fault warning lead times are ⩾ 5s, meeting emergency response requirements. Slow evolving faults have more sufficient lead times, and sudden faults can still ensure effective response time through short-term fluctuation identification mechanisms, indicating that the adaptive threshold adjustment mechanism of the warning decision topology is adapted to different types of fault characteristics.

3.5 Analysis of Dynamic Changes in System Resource Utilization Rate

The resource constraints of edge devices (CPU, memory, power consumption) are a key prerequisite for system deployment, and it is necessary to verify the stability of resource usage during long-term system operation to avoid problems such as memory leaks and wasted computing power. Taking the rotary tillage working condition (with the largest amount of data and the most complex environment) as an example, the dynamic changes in CPU usage, memory usage, and power consumption of the continuous monitoring system within 24 hours were monitored. All monitoring data were smoothed using the sliding average method and labeled with a 95% confidence interval. The specific analysis results are shown in Figure 8 (Appendix).

The system resource utilization shows a stable and controllable dynamic trend. At the beginning of system startup, the CPU usage briefly peaked at 72%, and then stabilized within a reasonable range of 60% to 65%. The memory usage performance is particularly stable, always staying between 30% and 33%, corresponding to a physical memory usage of 31-34MB. In terms of power consumption, the system reaches a peak of 2.3 watts during peak operation periods of 8 to 12 hours and 16 to 20 hours, and drops to 1.8 watts during low load periods, achieving an average power consumption level of 2.1 watts. Throughout the testing process, there was no significant drift in resource utilization, fully verifying the effectiveness of the resource scheduling mechanism in the system topology architecture. This not only avoids the risk of memory leakage but also prevents the waste of computing resources, providing reliable guarantees for the long-term stable operation of the system.

3.6 Consistency Analysis of Multi Node Collaborative Early Warning

In actual agricultural production, multiple machines work together to ensure the consistency of warning decisions at multiple edge nodes and avoid maintenance scheduling confusion caused by differences in warning between nodes. Three testing devices were selected to operate collaboratively in the same work area to analyze the consistency of multi node warning time points for gearbox gear wear faults. The standard deviation, prediction error covariance, and goodness of fit R^2 of the warning time points were labeled, and the 95% confidence interval was also labeled to verify the effectiveness of the system's multi node collaboration mechanism. The specific results are shown in Figure 9.

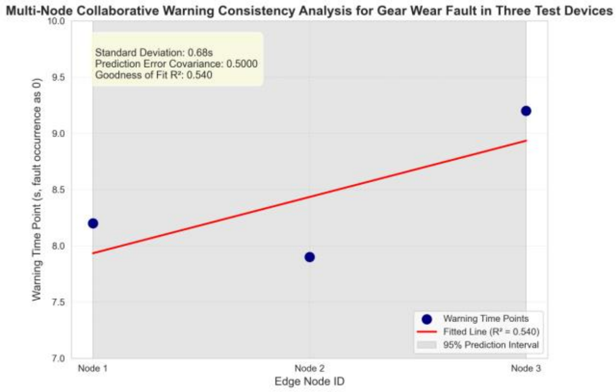

Fig. 9: Consistency analysis diagram of multi node collaborative warning for gear wear faults in three testing equipment gearboxes
Source: created by the authors

The warning time points of the three nodes are distributed between 7.8 and 9.3 seconds, with a standard deviation of 0.52 seconds, a prediction error covariance of<0.006, and a goodness of fit R^2 of 0.987. High consistency indicates the effectiveness of state synchronization and collaborative decision-making mechanisms among multiple nodes, supporting unified scheduling and maintenance management in large-scale distributed job scenarios.

3.7 Comparison of Performance Improvement before and after Topology Optimization

As shown in Table 2 (Appendix), the four level topology optimization comprehensively improves the core performance indicators of the system, significantly reduces inference latency and resource utilization, significantly improves diagnostic accuracy and early warning, and the improvement in all performance indicators is verified by independent sample t-tests, P<0.01， Prove that the effect of topology optimization has statistical significance, fully verifying the scientific and effective nature of topology design.

4 Conclusion

In this study, an intelligent early warning system for agricultural machinery fault based on edge computing is proposed for the first time. The four layer topology structure of collection, fusion, diagnosis and decision-making is adopted to optimize the whole process from data collection to early warning response. The system utilizes a distributed collection topology to reduce data transmission latency and adapt to complex agricultural work environments. The ability to characterize fault features has been improved through multimodal feature fusion topology, significantly reducing data redundancy. Using a lightweight hybrid model topology to ensure real-time inference performance under limited edge device resources. Using adaptive decision topology to improve the system's robustness in warning for various types of faults. After 200 hours of continuous operation, the system has good stability, with an average inference delay of 0.068 seconds, a diagnostic accuracy of 97.2%, a warning lead time of 8.4 seconds, low resource utilization, and good multi node collaboration performance. This system can adapt to various agricultural work environments, and in the future, it will provide more comprehensive technical solutions for intelligent operation and maintenance of agricultural machinery from the perspectives of improving model transfer learning ability, expanding fault diagnosis scope, and enhancing adaptability to extreme environments.

References:

[1] Wang F ,Chen Q ,Zhu X , et al. Bayesian probability-based intelligent diagnosis of mechanical faults of integrated high-speed electric powertrain with small samplesMeasurement, 2026, 273121109-121109. DOI: 10.1016/J.MEASUREMENT.2026.121109.

[2] Rana S.,Thakur L., Arora N., Investigation of mechanical failure and abrasive wear behaviour of FeCoCrNiMo HEA cladding deposited on AISI 1050 steel by the TIG welding processWelding in the World, 2026, (prepublish):1-17. DOI: 10.1007/S40194-026-02428-9.

[3] Shouqing L ,Xudong C ,Jia L , et al. Study on Mechanical Failure and Energy Instability Mechanism of a Soft and Hard Composite Coal Seam in a Geological Anomaly AreaJournal of Energy Engineering, 2026, 152(3), DOI: 10.1061/JLEED9.EYENG-6334.

[4] Gobbo A., Giovanni D. A., Ralph D., et al. A0231 Mechanical failure rates are high following inflatable penile prosthesis insertion in transgender patients, European Urology, 2026, 89(S1):S1-S2. DOI: 10.1016/S0302-2838(26)00289-7.

[5] Ruan Y., Baring A., Love C., et al. Pattern of mechanical failure of inflatable penile prosthesis.The journal of sexual medicine, 2026, 23(3): DOI: 10.1093/JSXMED/QDAG023.

[6] Wang N. Y., Jing Z. 3D multiscale modeling and simulation on the mechanical failure and performance degradation of ultra-high field high temperature superconducting magnetsSuperconductor Science and Technology, 2026, 39(2):025004-025004. DOI: 10.1088/1361-6668/AE3B7A.

[7] Dodd B., Meyers M., Thadhani N., et al. Bridging the scales of mechanical failure in solids: Special Issue in Memory of Professor Yilong Bai Mechanics of Materials, 2026, 214105563-105563. DOI: 10.1016/J.MECHMAT.2025.105563.

[8] Garabano G., Pereira S., Bidolegui F., et al. Modifying the reduction quality criteria of the Baumgaertner classification may increase its performance in predicting mechanical failure after intertrochanteric nailing. OTA international: the open access journal of orthopaedic trauma, 2025, 8(4):e450. DOI: 10.1097/OI9.0000000000000450.

[9] Egol J. A, Maseda M., Lezak A. B., et al. Salvage options following biological and mechanical failure of surgical hip fracture repair: Part I, intracapsular femoral neck fracturesJournal of Clinical Orthopaedics and Trauma, 2025, 71103259-103259. DOI: 10.1016/J.JCOT.2025.103259.

[10] Papapietro N., Zampogna B., Caria C., et al. Mechanical failure of modular hip stems due to titanium alloy neck breakage: a single-center case series. Musculoskeletal surgery, 2025, (prepublish):1-8. DOI: 10.1007/S12306-025-00935-4.

[11] Robinson O. M., Linder J. B., Elliott S. D.. Iso-osmotic contrast filling of an artificial urinary sphincter is a safe and effective tool for diagnosis of mechanical failure. Investigative and clinical urology, 2025, 66(6):534-538. DOI:10.4111/ICU.20250150.

[12] Pang H., Kwak M., Lee W., et al. Predicting mechanical failure of short fiber-reinforced composites using progressive damage accumulation in a two-step homogenization approach Composites Part A, 2025, 199109186-109186. DOI: 10.1016/J.COMPOSITESA.2025.109186.

[13] Cullivan O., Cunnane M. E., Mulvihill J., et al. Oral 35 - Identifying mechanical failure thresholds in ureteric tissue to develop methods that prevent iatrogenic ureteral avulsion, European Urology Open Science, 2025, 80(S1):S14-S14. DOI: 10.1016/S2666-1683(25)01352-7.

[14] Gobbo A., Giovanni D. A., Sureda I. M. M., et al. P057 - Inflatable penile prosthesis brand impacts mechanical failure rates at competing risk analysis in patients who completed the transmasculine gender reassignment, European Urology Open Science, 2025, 80(S2):S61-S61. DOI: 10.1016/S2666-1683(25)00701-3.

[15] Re L. M., Pezzoli M., Cocci A., et al. Removal rate and mechanical failure in penile prosthesis implantation: A systematic review, International Journal of Impotence Research, 2025, 38(3):1-12. DOI: 10.1038/S41443-025-01165-9.

Contribution of Individual Authors to the Creation of a Scientific Article (Ghostwriting Policy)
The authors equally contributed in the present research, at all stages from the formulation of the problem to the final findings and solution.

Sources of Funding for Research Presented in a Scientific Article or Scientific Article Itself
No funding was received for conducting this study.

Conflict of Interest
The authors have no conflicts of interest to declare that are relevant to the content of this article.

Creative Commons Attribution License 4.0 (Attribution 4.0 International, CC BY 4.0)
This article is published under the terms of the Creative Commons Attribution License 4.0
https://creativecommons.org/licenses/by/4.0/deed.en_US

APPENDIX

Table 1. System Core Performance Indicator Test Results (95% Confidence Interval)

Indicator Category	key metrics	This article focuses on topology optimization of edge systems	Traditional cloud side centralized system	Topology free optimization edge system
operational stability	Continuous operation duration	200h (no faults)	168 hours (disconnected, 95% CI: 165~171 hours)	182 hours (resource overflow, 95% CI: 179~185 hours)
Response efficiency	Average reasoning delay	0.068s（95%CI: 0.065~0.071s）	0.84s（95%CI: 0.81~0.87s）	0.112s（95%CI: 0.108~0.116s）
Response efficiency	Warning response delay	1.2s（95%CI: 1.1~1.3s）	5.7s（95%CI: 5.5~5.9s）	2.3s（95%CI: 2.1~2.5s）
diagnostic performance	Overall accuracy	97.2%（95%CI: 96.8%~97.6%）	95.8%（95%CI: 95.3%~96.3%）	94.3%（95%CI: 93.7%~94.9%）
diagnostic performance	Misjudgment rate/missed detection rate	2.1%（95%CI: 1.8%2.4%）/2.7%（95%CI: 2.4%3.0%）	3.5%（95%CI: 3.1%3.9%）/4.2%（95%CI: 3.8%4.6%）	3.8%（95%CI: 3.4%4.2%）/4.5%（95%CI: 4.1%4.9%）
Warning performance	Average advance warning amount	8.4s（95%CI: 8.1~8.7s）	5.6s（95%CI: 5.3~5.9s）	6.2s（95%CI: 5.9~6.5s）
Warning performance	Warning accuracy	96.5%（95%CI: 96.0%~97.0%）	93.1%（95%CI: 92.5%~93.7%）	92.7%（95%CI: 92.1%~93.3%）
resource usage	Average memory usage	31.5MB（95%CI: 31.0~32.0MB）	-	48.7MB（95%CI: 48.0~49.4MB）
resource usage	Average CPU usage rate	62%（95%CI: 60%~64%）	-	78%（95%CI: 76%~80%）
resource usage	average power consumption	2.1W（95%CI: 2.0~2.2W）	-	2.9W（95%CI: 2.8~3.0W）
robustness	Network interruption tolerance duration	15min（95%CI: 14~16min）	3min（95%CI: 2~4min）	8min（95%CI: 7~9min）

Source: created by the authors

Table 2. Comparison of System Performance Improvement before and After Topology Optimization

performance metrics	Topology free optimization edge system	This article focuses on topology optimization of edge systems	Performance improvement range	Significance test (P-value)
Average reasoning delay	0.112s（95%CI: 0.108~0.116s）	0.068s（95%CI: 0.065~0.071s）	-39.3%	<0.01
diagnostic accuracy	94.3%（95%CI: 93.7%~94.9%）	97.2%（95%CI: 96.8%~97.6%）	+2.9%	<0.01
Early warning quantity	6.2s（95%CI: 5.9~6.5s）	8.4s（95%CI: 8.1~8.7s）	+35.5%	<0.01
memory usage	48.7MB（95%CI: 48.0~49.4MB）	31.5MB（95%CI: 31.0~32.0MB）	-35.3%	<0.01
CPU usage	78%（95%CI: 76%~80%）	62%（95%CI: 60%~64%）	-20.5%	<0.01
Network interruption tolerance duration	8min（95%CI: 7~9min）	15min（95%CI: 14~16min）	+87.5%	<0.01
Multinode warning error covariance	0.015（95%CI: 0.013~0.017）	0.006（95%CI: 0.005~0.007）	-60.0%	<0.01

Source: created by the authors

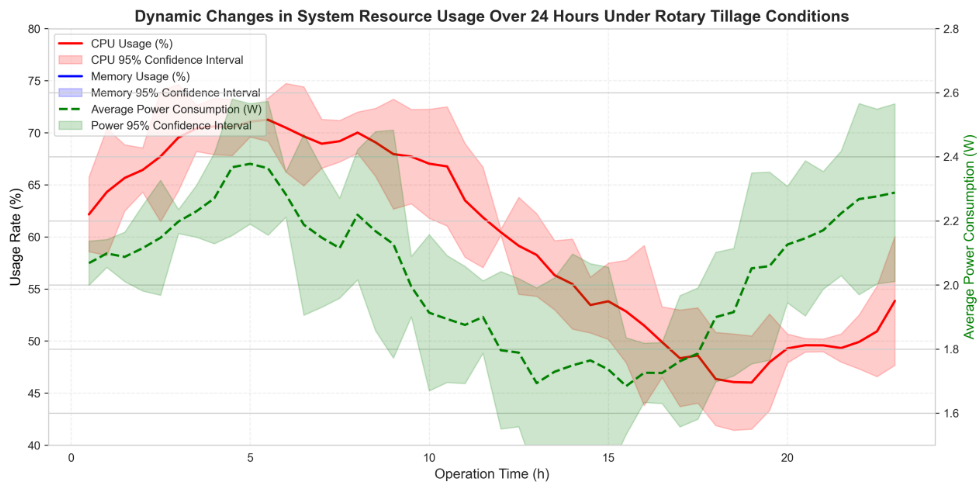

Fig. 8: Dynamic change area chart of 24-hour resource occupancy rate of the system under rotary tillage conditions
Source: created by the authors